

## Supporting Informations

### **Chromogenic and fluorogenic “off-on-off” chemosensor for selective and sensitive detection of aluminum ( $\text{Al}^{3+}$ ) and bifluoride ( $\text{HF}_2^-$ ) ions in solution and in living HepG2 cells: synthesis, experimental and theoretical studies**

Samit Pramanik,<sup>a</sup> Saikat Kumar Manna,<sup>b</sup> Sudipta Pathak,<sup>b,\*</sup> Debasish Mondal,<sup>c</sup> Kunal Pal,<sup>d</sup> and Subrata Mukhopadhyay<sup>a</sup>

<sup>a</sup>Department of Chemistry, Jadavpur University, Jadavpur, Kolkata, West Bengal, India

<sup>b</sup>Department of Chemistry, Haldia Government College, Debhog, Purba Medinipur, West Bengal, India

<sup>c</sup>School of Chemistry and Biochemistry, Thapar Institute of Engineering and Technology, Patiala-147004, Punjab, India

<sup>d</sup>Department of Life Science and Biotechnology, Jadavpur University, Kolkata 700032, India

\*Sudipta Pathak, Tel:+91-8001317336

E-mail: sudiptachemster@gmail.com

**Table of contents:**

Sl. No.	Contents	Page No.
1.	Table S1 Comparative study	3–4
2.	Fig. S1 $^1\text{H}$ NMR spectrum of <b>L</b> in DMSO- $d_6$ solution	4
3.	Fig. S2 $^{13}\text{C}$ NMR spectrum of <b>L</b> in DMSO- $d_6$ solution	5
4.	Fig. S3 ESI-mass spectrum of <b>L</b>	5
5.	Fig. S4 FT-IR spectrum of <b>L</b>	6
6.	Table S2 Single Crystal X-ray diffraction data of <b>L</b>	6–7
7.	Table S3 Some important bond length and bond angles of <b>L</b>	7–8
8.	Fig. S5 $^1\text{H}$ NMR of <b>L-Al</b> $^{3+}$ complex in DMSO- $d_6$	8
9.	Fig. S6 FT-IR spectrum of <b>L-Al</b> $^{3+}$ complex	8
10.	Fig. S7 Reversible changes in fluorescence intensity of probe <b>L</b>	9
11.	Fig. S8 Plot of the fluorescence intensity at 476 nm versus the concentration of $\text{HF}_2^-$	9
12.	Fig. S9 Changes in the absorption spectra of <b>L-2Al</b> $^{3+}$ complex in presence of different anions	9
13.	Fig. S10 Fluorescence Job's plot for <b>L</b> with $\text{Al}^{3+}$	10
14.	Fig. S11 Calculation for Limit of Detection (LOD)	10
15.	Fig. S12 Binding constant calculation	11
16.	Computational details	11–12
17.	Table S4 Energies of the highest occupied molecular orbital (HOMO) and lowest unoccupied molecular orbital (LUMO)	12
18.	Table S5 Energies of the important molecular orbitals in au	12
19.	Table S6 Calculated excitation energies (eV), oscillator strengths (f), contributions for Al-complex	13
20.	Fig. S13 Molecular orbital plots of <b>L</b> and <b>L-2Al</b> $^{3+}$	14
21.	Optimized coordinates of <b>L</b> and <b>L-2Al</b> $^{3+}$	15–17
22.	Fig. S14 Cell survivability assay	17
23.	Fig. S15 Influence of pH on absorbance ratio ( $A_{402}/A_{345}$ ) of <b>L</b> in the absence and presence of $\text{Al}^{3+}$	18
24.	Fig. S16 Fluorescence emission (at $\lambda_{\text{max}} = 476$ nm) spectral changes of <b>L</b> and <b>L+Al</b> $^{3+}$ complex with pH variation	18

**Table S1.** Summary of representative fluorescent probes for Al<sup>3+</sup>

Paper	Al <sup>3+</sup> detection limit	Interferences (cation/anion)	Any other remark	Our work
1. S. K. Sheet, B. Sen, R. Thounaojam, K. Aguan and S. Khatua, <i>J. Photochem. Photobiol., A</i> , 2017, <b>332</b> , 101.	1.62 μM	PPi (Inorganic pyrophosphate)	Starting materials are not readily available.	Starting materials are commercially available. There is no interference from a number of cations.
2. S. Samanta, U. Manna, T. Ray and G. Das, <i>Dalton Trans.</i> , 2015, <b>44</b> , 18902.	$6.86 \times 10^{-7}$ M	No	Starting materials are not readily available.	Starting materials are commercially available.
3. O. Alici and S. Erdemir, <i>Sens. Actuators, B</i> , 2015, <b>208</b> , 159.	$(13.7 \pm 0.17) \times 10^{-7}$ M	No	Starting materials are not readily available.	Starting materials are commercially available.
4. D. Maity and T. Govindaraju, <i>Chem. Commun.</i> , 2010, <b>46</b> , 4499.	Not reported	Cu <sup>2+</sup> , In <sup>3+</sup>	Starting materials are not readily available.	There is no interference from a number of cations.
5. J. C. Qin, T. R. Li, B. D. Wang, Z. Y. Yang and L. Fan, <i>Spectrochim. Acta, Part A</i> , 2014, <b>133</b> , 38.	$8.2 \times 10^{-7}$ M	No	Multistep reaction.	Comparatively less reaction steps.
6. R. Patil, A. Moirangthem, R. Butcher, N. Singh, A. Basu, K. Tayade, U. Fegade, D. Hundiwale and A. Kuwar, <i>Dalton Trans.</i> , 2014, <b>43</b> , 2895.	$4.2 \times 10^{-5}$ M	No	Starting materials are commercially available.	LOD is 0.8 μM
7. S. Malkondu, <i>Tetrahedron</i> , 2014, <b>35</b> , 5580.	0.33 μM	Fe <sup>3+</sup> , Hg <sup>2+</sup> , Pb <sup>2+</sup> , and Zn <sup>2+</sup>	Starting materials are not readily available.	There is no interference from a number of cations.
8. V. K. Gupta, A. K. Singh and L. K. Kumawat, <i>Sens. Actuators, B</i> , 2014, <b>195</b> , 98.	$1.0 \times 10^{-6}$ M	Ni <sup>2+</sup>	Starting materials are commercially available.	There is no interference from a number of cations. LOD is 0.8 μM
9. S. Erdemir and S. Malkondu, <i>J. Lumin.</i> , 2015, <b>158</b> , 401.	$(9.82 \pm 0.27) \times 10^{-6}$ M	No	Starting materials are commercially available.	LOD is 0.8 μM
10. S. Mukherjee, P. Mal and H. Stoeckli-Evans, <i>J. Lumin.</i> , 2016, <b>172</b> , 124.	0.08 μM	Cu <sup>2+</sup> , Fe <sup>2+</sup> and Fe <sup>3+</sup>	Starting materials are commercially available.	There is no interference from a number of cations.

11. S. Lia, D. Caoa, X. Mengc, Z. Hua, Z. Lia, C. Yuana, T. Zhoua, X. Hana and W. Maa, <i>J. Photochem. Photobiol. A</i> , 2020, <b>392</b> , 112427.	0.16 $\mu\text{M}$	No	Multistep reaction.	Comparatively less reaction steps.
12. Y. -l. Mua, C. -j. Zhang, Z. -l. Gaoa, X. Zhang, Q. Lu, J. -s. Yaoa and S. Xing, <i>Synth. Met.</i> , 2020, <b>262</b> , 116334.	$2 \times 10^{-6} \text{ M}$	No	Starting materials are not commercially available.	Starting materials are commercially available. LOD is 0.8 $\mu\text{M}$
13. V. Saini, K. Ranganb and B. Khungar, <i>Photochem. Photobiol. Sci.</i> , 2020, DOI: 10.1039/C9PP00477G	54 nM	No	Starting materials are not commercially available.	Starting materials are commercially available.

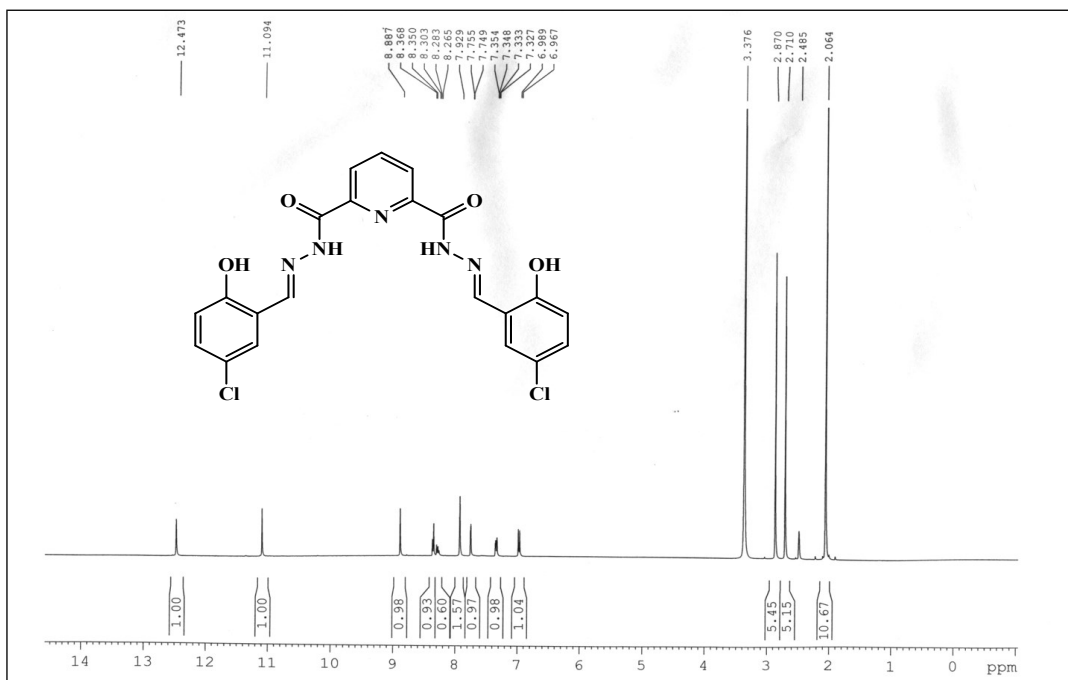
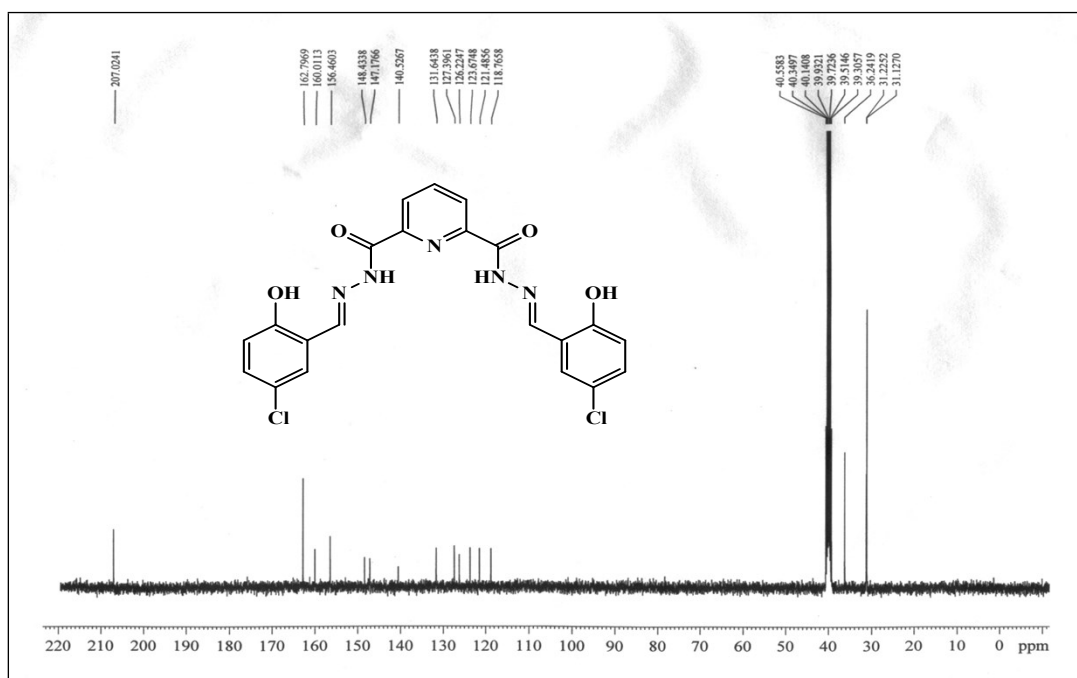
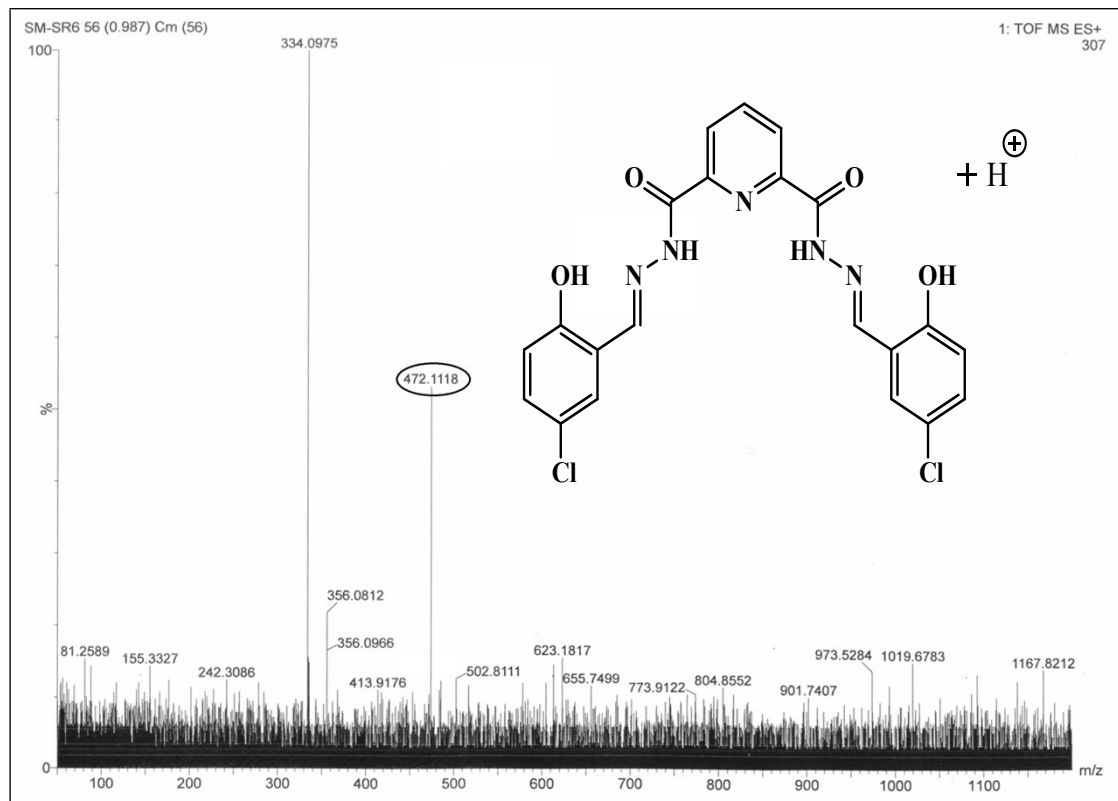


Fig. S1  $^1\text{H}$  NMR spectrum of **L** in  $\text{DMSO}-d_6$  solution



**Fig. S2**  $^{13}\text{C}$  NMR spectrum of **L** in  $\text{DMSO}-d_6$  solution



**Fig. S3** ESI-mass spectrum of **L**

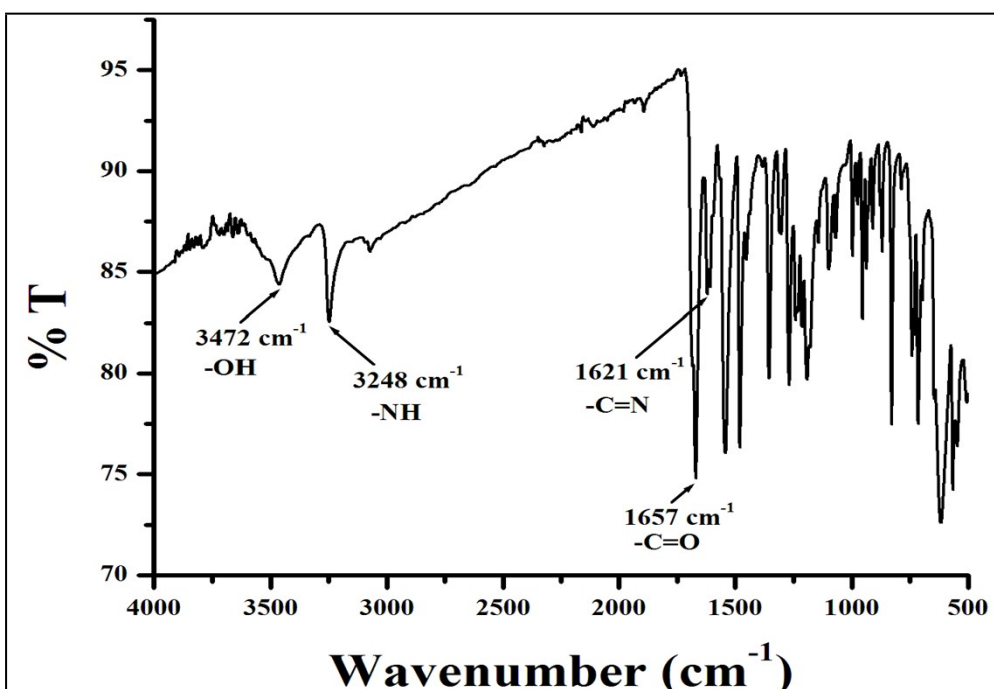


Fig. S4 FT-IR spectrum of **L**

**Table S2** Single Crystal X-ray diffraction data of sensor **L**

Structure	Sensor, <b>L</b>
CCDC number	1979155
Empirical formula	C <sub>48</sub> H <sub>46</sub> Cl <sub>4</sub> N <sub>12</sub> O <sub>12</sub>
Formula Weight	1124.77
Temperature (K)	273(2)
Wavelength (Å)	0.71073
Crystal system	Triclinic
space group	P-1
a, b, c (Å)	13.8336(11), 14.4635(11), 15.3548(12)
α, β, γ (°)	66.622(2), 71.512(2), 85.747(3)
Volume (Å <sup>3</sup> )	2669.8(4)
Z / Density (calc.) (Mg/m <sup>3</sup> )	2 / 1.399
Absorption coefficient (mm <sup>-1</sup> )	0.293
F(000)	1164.0
Crystal size (mm <sup>3</sup> )	0.08 × 0.13 × 0.19
θ range for data collection	1.802 to 27.121

Completeness to $\theta$ (%)	100%
Absorption correction	multi-scan
Max. and min. transmission	0.977 and 0.955
Refinement method	Full-matrix least-squares on $F^2$
Data/parameters	11722/ 753
Goodness-of-fit on $F^2$	1.110
Final R indices [ $I > 2\sigma(I)$ ]	$R_1 = 0.0534, wR_2 = 0.1636$
R indices (all data)	$R_1 = 0.0765, wR_2 = 0.1886$
Largest diff. peak and hole ( $\text{\AA}^{-3}$ )	0.780 and -0.588

$R_1 = \sum ||F_o| - |F_c|| / \sum |F_o|, wR_2 = [\sum \{(F_o^2 - F_c^2)^2\} / \sum \{w(F_o^2)^2\}]^{1/2} w = 1/\{\sigma^2(F_o^2) + (aP)^2 + bP\}$   
where,  $a = 0.1000$  and  $b = 0.6180$ .  $P = (F_o^2 + 2F_c^2)/3$

**Table S3** Some important bond length and bond angles of **L**

Bond	Length ( $\text{\AA}$ )	Bond	Angle ( $^\circ$ )
Cl (1)–C (18)	1.739(3)	C(1)–O(1)–H(1)	112(2)
Cl(2)–C(4)	1.736(3)	C(21)–O(4)–H(15)	110(3)
O(1)–C(1)	1.363(3)	N(2)–N(1)–C(15)	117.69(19)
O(2)–C(8)	1.216(3)	N(1)–N(2)–C(14)	118.93(19)
O(3)–C(14)	1.220(3)	N(5)–N(4)–C(8)	118.6(2)
O(4)–C(21)	1.351(3)	N(4)–N(5)–C(7)	118.17(19)
O(1)–H(1)	0.82(3)	N(1)–N(2)–H(10)	119(2)
O(4)–H(15)	0.90(4)	C(14)–N(2)–H(10)	123(2)
N(1)–N(2)	1.374(3)	N(5)–N(4)–H(6)	120(2)
N(1)–C(15)	1.273(3)	C(8)–N(4)–H(6)	120(2)
N(2)–C(14)	1.347(3)	O(1)–C(1)–C(6)	122.0(2)
N(4)–N(5)	1.359(3)	O(1)–C(1)–C(2)	118.2(2)
N(4)–C(8)	1.356(4)	O(2)–C(8)–N(4)	123.6(2)
N(5)–C(7)	1.279(3)	O(3)–C(14)–N(2)	123.3(2)

N(2)–H(10)	0.80(3)	O(2)–C(8)–C(9)	122.2(2)
N(4)–H(6)	0.72(2)	O(3)–C(14)–C(13)	122.1(2)
C(7)–H(5)	0.99(3)		
C(15)–H(11)	0.93(3)		

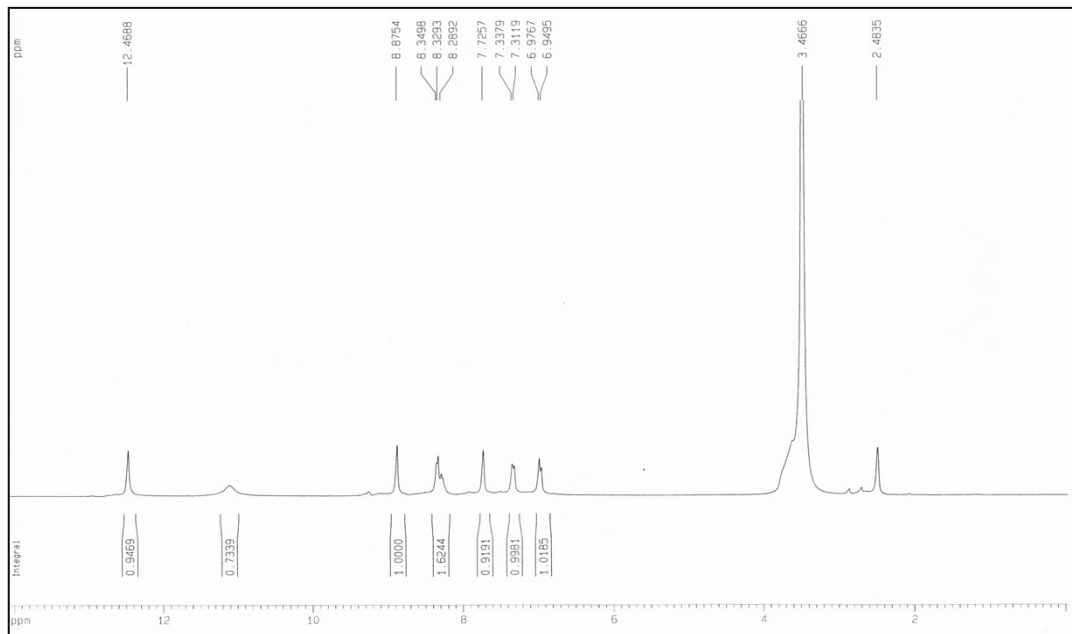


**Fig. S5**  $^1\text{H}$  NMR of  $\text{L}-2\text{Al}^{3+}$  complex in  $\text{DMSO-d}_6$

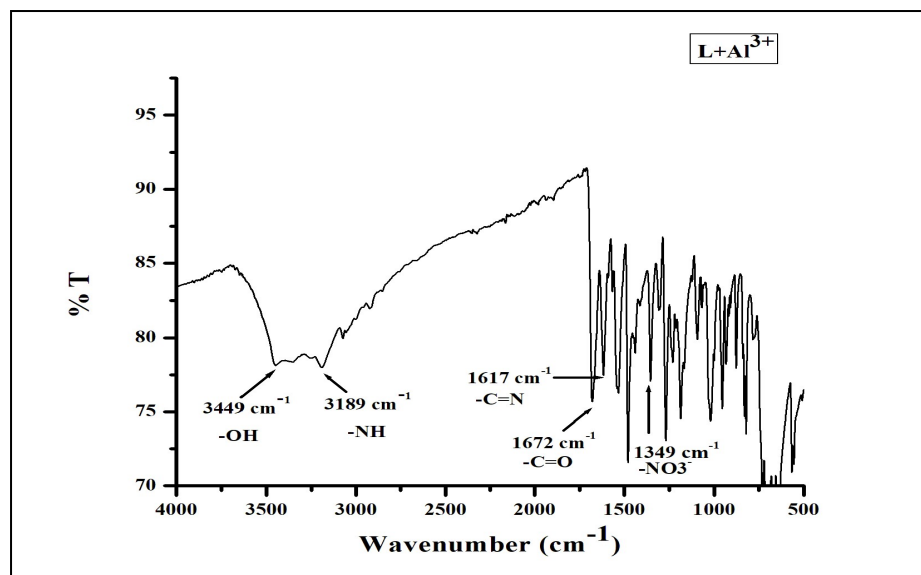


**Fig. S6** FT-IR spectrum of  $\text{L}-\text{Al}^{3+}$  complex

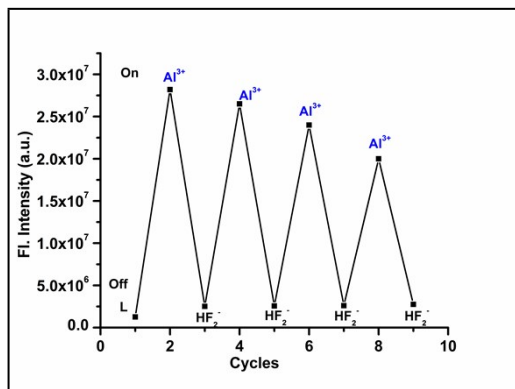


**Fig. S7** Reversible changes in fluorescence intensity of probe **L** at 476 nm (DMSO-H<sub>2</sub>O, 8:2, v/v, 10 mM HEPES buffer, pH 7.4) upon alternate addition of  $\text{Al}^{3+}$  and  $\text{HF}_2^-$  solution upto four cycles

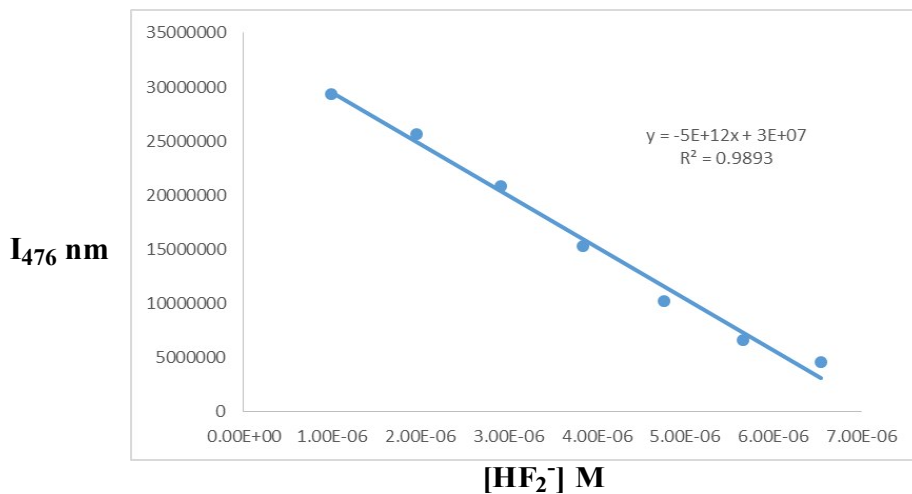


**Fig. S8** Plot of the fluorescence intensity at 476 nm versus the concentration of  $\text{HF}_2^-$

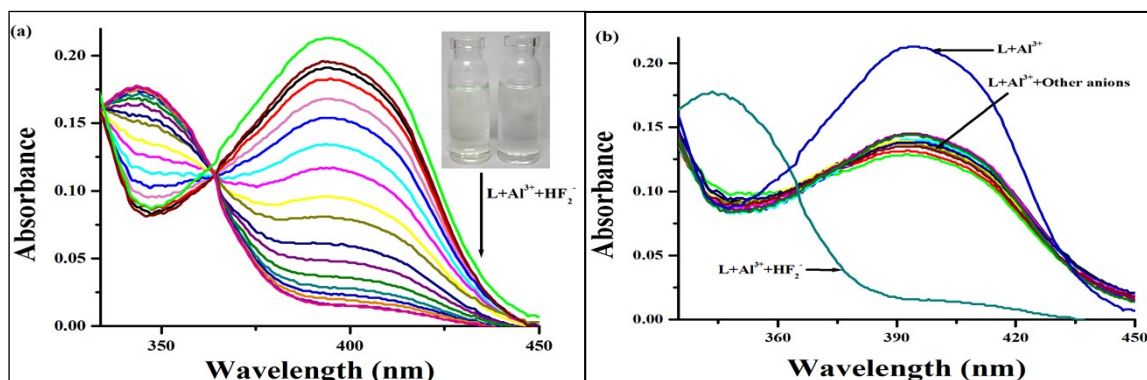


**Fig. S9** (a) UV-vis absorption spectra of **L**- $2\text{Al}^{3+}$  complex with sodium salt of bifluoride in DMSO-H<sub>2</sub>O (8:2, v/v, 10 mM HEPES buffer, pH 7.4) solution. Inset: Color change after addition of  $\text{HF}_2^-$  to  $\text{L}+\text{Al}^{3+}$ . (b) Changes in the absorption spectra of **L**- $2\text{Al}^{3+}$  complex in presence of different anions.

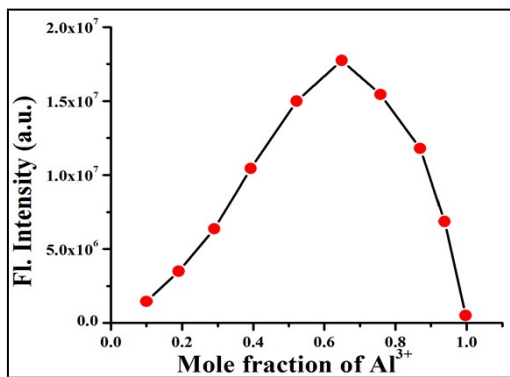


**Fig. S10** Fluorescence Job's plot for **L** with  $\text{Al}^{3+}$  in DMSO/ $\text{H}_2\text{O}$  solution (8:2, v/v, 10 mM HEPES buffer, pH 7.4). ( $[\text{H}] = [\text{G}] = 4 \times 10^{-5}$  M)

#### Calculation for detection limit:

The detection limit of **L** for  $\text{Al}^{3+}$  was determined using the following equation: Detection limit =  $3S_{\text{bl}}/S$ ,  $S_{\text{bl}}$  is the standard deviation of the blank solution;  $S$  is the slope of the calibration curve.

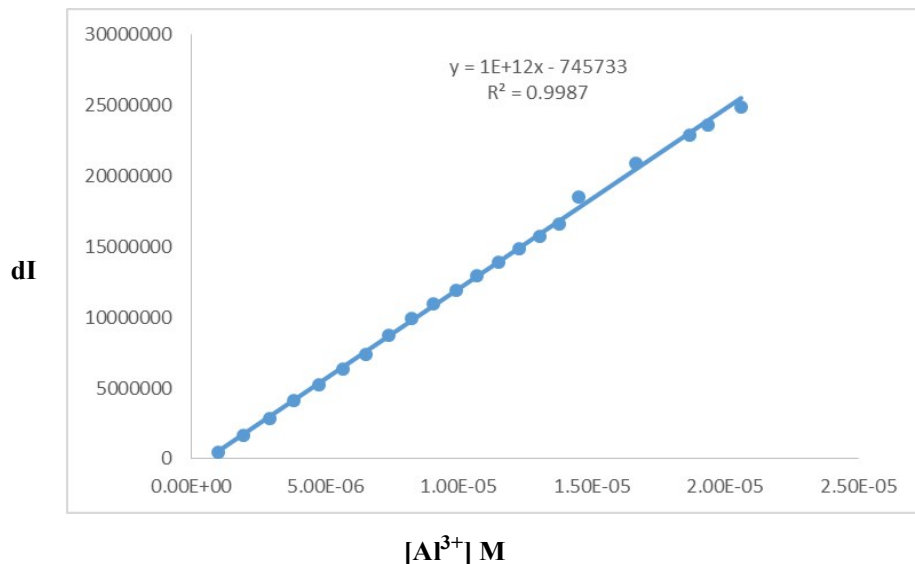


**Fig. S11** Calibration curve for fluorescence titration of **L** with  $\text{Al}^{3+}$

From the graph we get slope ( $S$ ) =  $1 \times 10^{12}$  Standard deviation ( $S_{\text{bl}} = 274989.74356$ ) Thus, using the formula, we get the detection limit =  $0.8249 \times 10^{-6}$  M =  $0.8249 \mu\text{M} = 8.2 \times 10^{-7}$  M.

### Binding constant calculation:

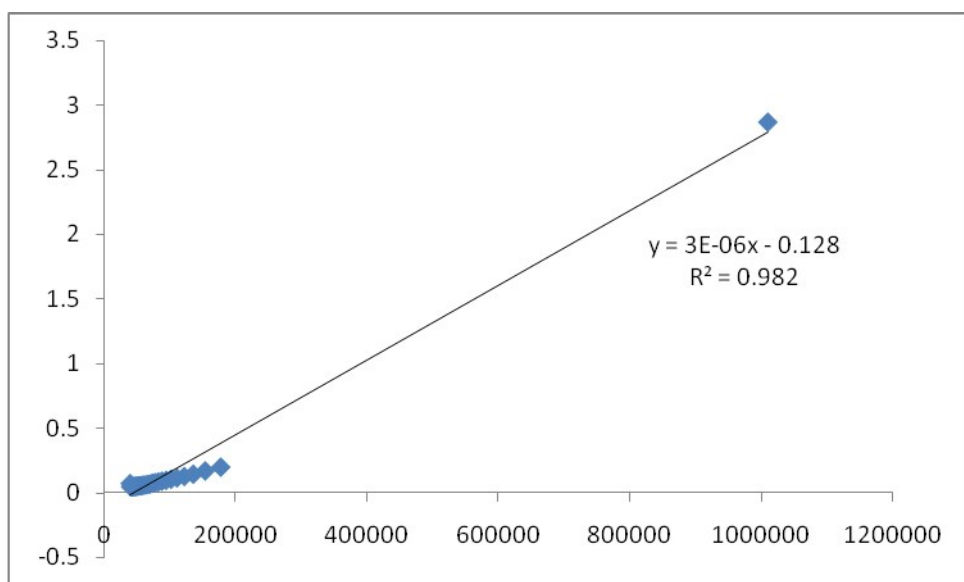


**Fig. S12** Bensei-Hildebrand plot obtained from the Fluorescence (emission calculated from 478 nm) studies. Binding constant ( $K_a = 4.26 \times 10^4 \text{ M}^{-1}$ ) curve of sensor **L** with  $\text{Al}^{3+}$  determined by fluorescence method.

### Computational Details:

All the geometries for **L** and **L**- $2\text{Al}^{3+}$  were optimized by using density functional theory (DFT) at the Becke's three-parameter hybrid exchange functional and the Lee–Yang–Parr correlation functional (B3LYP)<sup>1-3</sup> in combination with Pople's split-valence basis set 6-31+G(d, p) basis set<sup>4</sup>. Harmonic vibrational frequencies also computed to confirm the optimized structures as local minima (no imaginary frequency). The effect of solvent (dimethyl sulfoxide) were considered by using self-consistent reaction field (SCRF) procedure with the integral equation formalism polarized continuum model (IEF-PCM).<sup>5-9</sup> Time dependent DFT calculation were also conducted at the same level of theory specifying the keyword TD (N states = 50, root = 1).<sup>10-11</sup> All the computations have been carried out in Gaussian 16 program.<sup>12</sup>

1. A. D. J. Becke, *Chem. Phys.*, 1993, **98**, 5648–5662.
2. C. T. Lee, W. T. Yang, and R. G. Parr, *Phys. Rev. B*, 1988, **37**, 785–789.
3. B. Miehlich, A. Savin, H. Stoll, and H. Preuss, *Chem. Phys. Lett.*, 1989, **157**, 200–206.
4. J. D. Dill, and J. A. J. Pople, *Chem. Phys.*, 1975, **62**, 2921–2923.
5. J. Tomasi, and M. Persico, *Chem. Rev.*, 1994, **94**, 2027–2094.
6. M. Cossi, V. Barone, R. Cammi, and J. Tomasi, *Chem. Phys. Lett.*, 1996, **255**, 327–335.
7. V. Barone, M. Cossi, and J. Tomasi, *J. Chem. Phys.*, 1997, **107**, 3210–3221.
8. V. Barone, M. Cossi, and J. Tomasi, *J. Comput. Chem.*, 1998, **19**, 404–417.
9. M. Cossi, and V. Barone, *J. Chem. Phys.*, 1998, **109**, 6246–6254.
10. R. Bauernschmitt and R. Ahlrichs, *Chem. Phys. Lett.*, 1996, **256**, 454–64.
11. R. E. Stratmann, G. E. Scuseria, and M. J. Frisch, *J. Chem. Phys.*, 1998, **109**, 8218–24.
12. Gaussian 16, Revision C.01, M. J. Frisch, G. W. Trucks, H. B. Schlegel, G. E. Scuseria, M. A. Robb, J. R. Cheeseman, G. Scalmani, V. Barone, G. A. Petersson, H. Nakatsuji, X. Li, M. Caricato, A. V. Marenich, J. Bloino, B. G. Janesko, R. Gomperts, B. Mennucci, H. P. Hratchian,

J. V. Ortiz, A. F. Izmaylov, J. L. Sonnenberg, -Y. D. Williams, F. Ding, F. Lipparini, F. Egidi, J. Goings, B. Peng, A. Petrone, T. Henderson, D. Ranasinghe, V. G. Zakrzewski, J. Gao, N. Rega, G. Zheng, W. Liang, M. Hada, M. Ehara, K. Toyota, R. Fukuda, J. Hasegawa, M. Ishida, T. Nakajima, Y. Honda, O. Kitao, H. Nakai, T. Vreven, K. Throssell, J. A. Jr. Montgomery, J. E. Peralta, F. Ogliaro, M. J. Bearpark, J. J. Heyd, E. N. Brothers, K. N. Kudin, V. N. Staroverov, T. A. Keith, R. Kobayashi, J. Normand, K. Raghavachari, A. P. Rendell, J. C. Burant, S. S. Iyengar, J. Tomasi, M. Cossi, J. M. Millam, M. Klene, C. Adamo, R. Cammi, J. W. Ochterski, R. L. Martin, K. Morokuma, O. Farkas, J. B. Foresman, D. J. Fox, Gaussian, Inc., Wallingford CT, 2016.

**Table S4.** Energies of the highest occupied molecular orbital (HOMO) and lowest unoccupied molecular orbital (LUMO)

Species	E <sub>HOMO</sub> (a.u)	E <sub>LUMO</sub> (a.u)	ΔE(a.u)	ΔE(eV)	ΔE(kcal/mol)
<b>L</b>	-0.23351	-0.0926	0.14091	3.83	88.4
<b>L-2Al<sup>3+</sup></b>	-0.22925	-0.11303	0.11622	3.16	72.9

**Table S5.** Energies of the important molecular orbitals in au

Orbital	L	L-2Al <sup>3+</sup>
HOMO	-0.23351	-0.22925
HOMO-1	-0.23352	-0.23089
HOMO-2	-0.25807	-0.25262
LUMO	-0.09260	-0.11303
LUMO-1	-0.09004	-0.11272
LUMO-2	-0.06651	-0.08224

**Table S6.** Calculated excitation energies (eV), oscillator strengths (f), contributions for Al-complex. The data were calculated by the TDDFT//B3LYP/6-31+G(*d,p*) level of theory based on the optimized ground state geometries.

Species	Electronic Transition	Excitation Energy	f	Contributions
<b>L</b>	$S_0 \rightarrow S_1$	3.1938 eV 388.21 nm	0.2353	HOMO → LUMO (64%) HOMO-3 → LUMO+1 (31%)
	$S_0 \rightarrow S_7$	3.9695 eV 312.34 nm	0.2148	HOMO -4 → LUMO (69%)
<b>L-2Al<sup>3+</sup></b>	$S_0 \rightarrow S_1$	2.6986 eV 459.44 nm	0.2646	HOMO → LUMO (49%) HOMO → LUMO+1 (32%)
	$S_0 \rightarrow S_{10}$	3.7387 eV 331.62 nm	0.3280	HOMO-3 → LUMO (58%)
	$S_0 \rightarrow S_{15}$	3.8651 eV 320.78 nm	0.4837	HOMO-3 → LUMO+1 (41%)

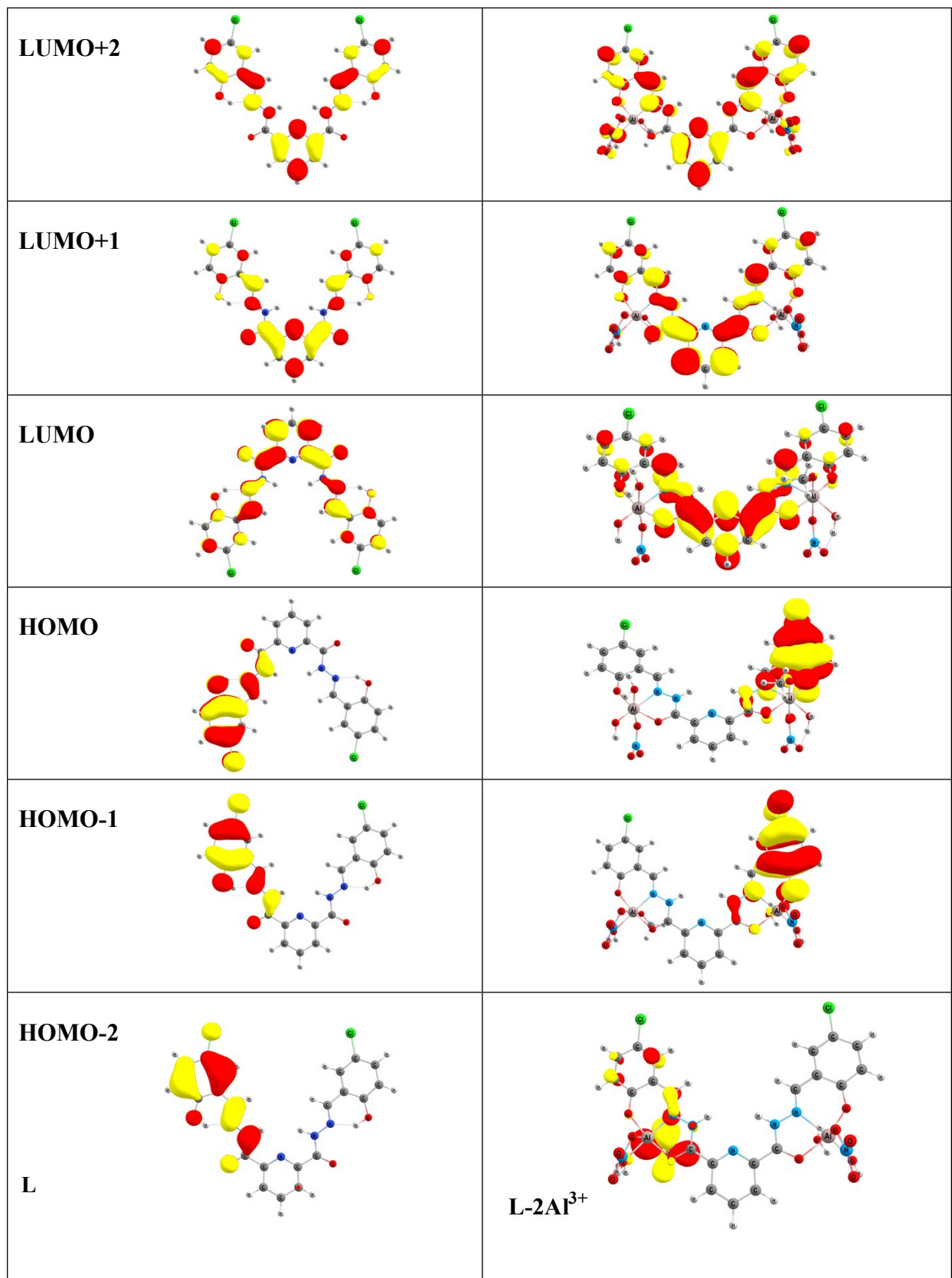


**Figure S13:** Molecular orbital plots of **L** and **L–2Al<sup>3+</sup>**

**Optimized Coordinates:**

**L**

C	-1.197844000	-5.389224000	-0.001934000
C	-1.148112000	-3.990834000	-0.001571000
N	0.002832000	-3.302113000	-0.002790000
C	1.153681000	-3.990893000	-0.002115000
C	1.203474000	-5.389259000	-0.002354000
C	0.002792000	-6.096593000	-0.002834000
C	-2.443812000	-3.219019000	0.001308000
C	2.449392000	-3.218810000	0.000210000
O	3.544264000	-3.780738000	0.009696000
O	-3.538441000	-3.781541000	0.010085000
N	-2.286511000	-1.862251000	-0.005351000
N	2.291238000	-1.862182000	-0.007444000
N	3.373965000	-1.040511000	-0.002037000
N	-3.370254000	-1.042068000	-0.000642000
C	3.174984000	0.236539000	-0.007230000
C	-3.173684000	0.235362000	-0.004304000
C	-4.299855000	1.155414000	-0.000608000
C	4.299051000	1.158922000	-0.001780000
C	-4.045554000	2.541770000	-0.000480000
C	-5.098029000	3.443999000	0.001039000
C	-6.425553000	3.000661000	0.002936000
C	-6.692008000	1.634874000	0.002917000
C	-5.646649000	0.701868000	0.001779000
C	4.041558000	2.544546000	-0.003611000
C	5.091902000	3.449283000	-0.000144000
C	6.420355000	3.008890000	0.005339000
C	6.689931000	1.643616000	0.007219000
C	5.646737000	0.708330000	0.004148000
Cl	4.750686000	5.180656000	-0.003135000
O	5.968158000	-0.604922000	0.005898000
H	-2.158574000	-5.888837000	-0.001684000
H	2.164379000	-5.888895000	-0.002937000
H	0.002656000	-7.181404000	-0.002904000
H	-1.343695000	-1.480433000	-0.011012000
H	1.347871000	-1.481366000	-0.014049000
H	2.166228000	0.659945000	-0.015428000

H	-2.165776000	0.660788000	-0.009933000
H	-7.241359000	3.714933000	0.003453000
H	3.014927000	2.896045000	-0.007931000
H	7.234558000	3.725182000	0.007486000
H	7.713705000	1.284327000	0.011399000
H	5.130654000	-1.134942000	0.003310000
O	-5.964973000	-0.612139000	0.001677000
H	-5.125973000	-1.139695000	0.000334000
H	-3.019686000	2.895763000	-0.002107000
Cl	-4.760826000	5.176229000	0.000754000
H	-7.715027000	1.273473000	0.003912000

### L-2Al<sup>3+</sup>

C	-1.196197000	-4.020396000	-0.599064000
C	-1.107226000	-2.625294000	-0.514046000
N	0.052933000	-1.959460000	-0.473309000
C	1.180556000	-2.679119000	-0.518989000
C	1.204329000	-4.076672000	-0.602502000
C	-0.012601000	-4.754608000	-0.642014000
C	-2.348482000	-1.812628000	-0.463117000
C	2.457978000	-1.924019000	-0.478874000
O	3.578819000	-2.497922000	-0.496046000
O	-3.493298000	-2.334578000	-0.542587000
N	-2.239985000	-0.484381000	-0.326999000
N	2.410734000	-0.588394000	-0.422152000
N	3.634100000	0.036269000	-0.381926000
N	-3.431030000	0.196262000	-0.271303000
C	3.666132000	1.332330000	-0.262546000
C	-3.424963000	1.485056000	-0.096963000
C	-4.631411000	2.252222000	0.003613000
C	4.888568000	2.075259000	-0.214830000
C	-4.503461000	3.655687000	0.158273000
C	-5.626748000	4.445316000	0.281412000
C	-6.911382000	3.871238000	0.260460000
C	-7.054893000	2.502263000	0.113262000
C	-5.932795000	1.647195000	-0.025183000
C	4.803570000	3.481903000	-0.062574000
C	5.953099000	4.241869000	-0.019236000
C	7.218325000	3.634795000	-0.128347000
C	7.317977000	2.262030000	-0.279946000
C	6.166696000	1.437364000	-0.326706000
Cl	5.847662000	5.992215000	0.172801000
O	6.310019000	0.143358000	-0.479993000
H	-2.166945000	-4.499744000	-0.627912000
H	2.151805000	-4.600357000	-0.634667000
H	-0.038187000	-5.836625000	-0.705733000
H	-1.339756000	-0.019949000	-0.242732000
H	1.532833000	-0.076905000	-0.413390000
H	2.727704000	1.884189000	-0.194480000
H	-2.472273000	2.009785000	-0.017953000

H	-7.788031000	4.502597000	0.360164000
H	3.828315000	3.950755000	0.019620000
H	8.115088000	4.244431000	-0.093143000
H	8.289781000	1.787291000	-0.365055000
O	-6.129489000	0.358730000	-0.161087000
H	-3.513427000	4.099629000	0.179046000
Cl	-5.462435000	6.191916000	0.469470000
H	-8.041816000	2.051908000	0.096590000
Al	-5.025669000	-1.049578000	-0.546654000
Al	5.204688000	-1.331672000	-0.443255000
O	6.368427000	-2.632861000	-0.773863000
H	6.384593000	-3.297790000	-0.073887000
O	5.002616000	-1.263320000	-2.494547000
H	5.326594000	-0.466827000	-2.942601000
H	5.574570000	-1.998846000	-2.776276000
N	5.248929000	-2.316254000	2.334551000
O	5.536373000	-3.442047000	1.896358000
O	5.082004000	-2.079284000	3.535830000
O	5.113056000	-1.311291000	1.506803000
N	-4.925891000	-2.330456000	2.294054000
O	-4.428019000	-2.280183000	3.418972000
O	-5.512847000	-3.371224000	1.878657000
O	-4.859454000	-1.292110000	1.533142000
C	-4.643290000	-1.819790000	-3.316180000
H	-4.930535000	-2.872456000	-3.154286000
H	-3.543982000	-1.792624000	-3.388887000
H	-5.042681000	-1.521439000	-4.295607000
O	-5.135059000	-0.958195000	-2.319267000
O	-6.341350000	-2.446685000	-0.369610000
H	-6.162833000	-3.014146000	0.438209000
H	-6.532509000	-2.993060000	-1.144751000

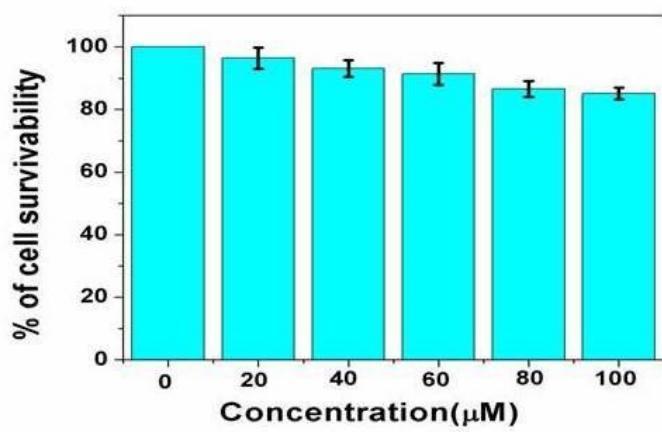


**Fig. S14** Cell survivability of WI-38 cells exposed to the ligand.

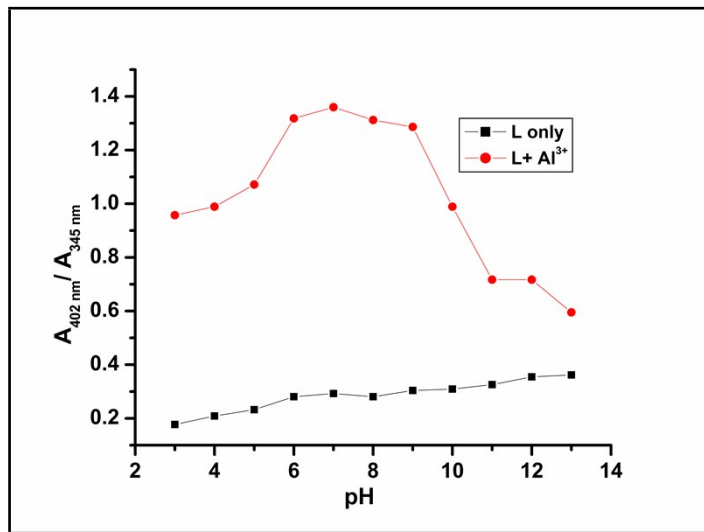


**Fig. S15** Influence of pH on absorbance ratio ( $A_{402}/A_{345}$ ) of **L** in the absence and presence of  $\text{Al}^{3+}$ .

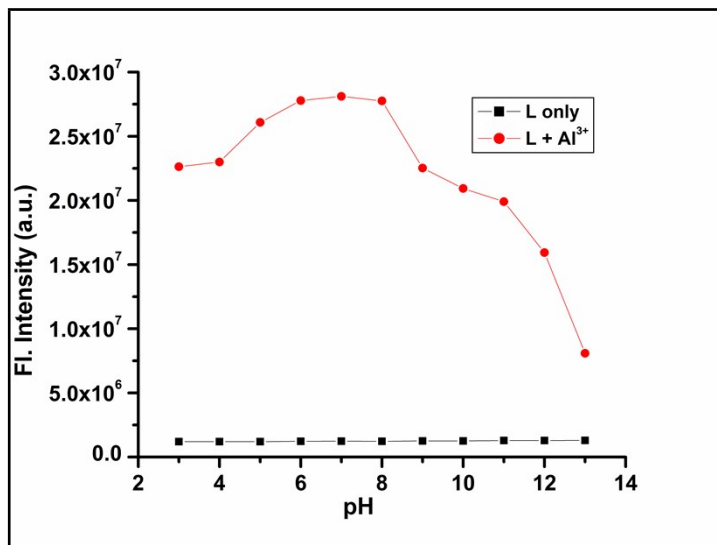


**Fig. S16** Fluorescence emission (at  $\lambda_{\text{max}} = 476$  nm) spectral changes of **L** and **L+Al<sup>3+</sup>** complex with pH variations.